J Neurophysiol 115: 413–422, 2016.
First published November 11, 2015; doi:10.1152/jn.00834.2015.

Chronic imaging of movement-related Purkinje cell calcium activity in awake behaving mice

Michael A. Gaffield,[1] Samantha B. Amat,[1] Haruhiko Bito,[2] and Jason M. Christie[1]
[1]*Max Planck Florida Institute for Neuroscience, Jupiter, Florida; and* [2]*Department of Neurochemistry, Graduate School of Medicine, The University of Tokyo, Tokyo, Japan*

Submitted 25 August 2015; accepted in final form 5 November 2015

Gaffield MA, Amat SB, Bito H, Christie JM. Chronic imaging of movement-related Purkinje cell calcium activity in awake behaving mice. *J Neurophysiol* 115: 413–422, 2016. First published November 11, 2015; doi:10.1152/jn.00834.2015.—Purkinje cells (PCs) are a major site of information integration and plasticity in the cerebellum, a brain region involved in motor task refinement. Thus PCs provide an ideal location for studying the mechanisms necessary for cerebellum-dependent motor learning. Increasingly, sophisticated behavior tasks, used in combination with genetic reporters and effectors of activity, have opened up the possibility of studying cerebellar circuits during voluntary movement at an unprecedented level of quantitation. However, current methods used to monitor PC activity do not take full advantage of these advances. For example, single-unit or multiunit electrode recordings, which provide excellent temporal information regarding electrical activity, only monitor a small population of cells and can be quite invasive. Bolus loading of cell-permeant calcium (Ca^{2+}) indicators is short-lived, requiring same-day imaging immediately after surgery and/or indicator injection. Genetically encoded Ca^{2+} indicators (GECIs) overcome many of these limits and have garnered considerable use in many neuron types but only limited use in PCs. Here we employed these indicators to monitor Ca^{2+} activity in PCs over several weeks. We could repeatedly image from the same cerebellar regions across multiple days and observed stable activity. We used chronic imaging to monitor PC activity in crus II, an area previously linked to licking behavior, and identified a region of increased activity at the onset of licking. We then monitored this same region after training tasks to initiate voluntary licking behavior in response to different sensory stimuli. In all cases, PC Ca^{2+} activity increased at the onset of rhythmic licking.

Purkinje cell; cerebellum; calcium

NEURONAL SIGNALING within cerebellar circuits is thought to play a major role in motor learning that guides coordinated movements. In the most prominent model of cerebellar function, such learning depends on the plastic reweighting of synaptic inputs on Purkinje cell (PC) dendrites (Albus 1971; Marr 1969). Specifically, climbing fibers projecting from the inferior olive evoke complex spikes in postsynaptic PCs resulting in long-term depression (LTD) at coincidently active parallel fiber-to-PC synapses, driving the plasticity necessary for error-driven associative learning (Ito et al. 1982). Thus substantial effort has been expended on understanding the link between this plasticity and learned aspects of motor-driven behavior. For example, LTD in PCs can affect conditioned eyeblink responses (Koekkoek et al. 2003; Ohtani et al. 2014; but see Welsh et al. 2005), spatial learning (Burguiere et al. 2005; Rochefort et al. 2011), adaptation of the horizontal optokinetic reflex (Wang et al. 2014), and smooth pursuit eye movements (Medina and Lisberger 2008). However, climbing fiber-driven LTD alone has failed to fully account for behavioral learning in many cases including adaptation of the vestibuloocular reflex or conditioned eyeblink responses (Ke et al. 2009; Kimpo et al. 2014; Ly et al. 2013; Schonewille et al. 2010, 2011; Tanaka et al. 2013; Wetmore et al. 2014). In addition, the olivo-cerebellar system may play a more general role in organizing motor control through temporal pattern generation (Jacobson et al. 2008). Merging these findings into an improved model of cerebellar function will require a more detailed exploration of movement behavior in animals likely requiring new methodological approaches for functional evaluation of cerebellar circuits, for example, using trained mice to perform skilled licking or whisking movements for a water reward while under restricted water intake (e.g., Guo et al. 2014).

Commonly used approaches for studying PC activity in vivo include single-unit or multiunit electrode recordings and bolus loading of cell-permeant Ca^{2+} indicator dyes. While electrodes have the advantage of recording fast changes in simple spike output, they typically damage the cell under observation and only a limited number of electrodes can be implanted at one time. This restricts recordings to a small subpopulation of cells during a single experimental session and causes increasing levels of damage the longer an area is studied. Acute neuropil injection of Ca^{2+} indicators presents two problems. First, bolus loading is not cell type specific; instead, dye indiscriminantly permeates most membranes, leading to labeling of off-target neurons and glia (Nimmerjahn et al. 2009; Sullivan et al. 2005). Second, labeling is not persistent; thus functional imaging must occur within hours of dye injection, often the day of cranial window installation surgery. This limits the imaging period to a short epoch and raises concerns about the state of astrocyte and microglia activity in the recently exposed brain (Holtmaat et al. 2009).

Genetically encoded Ca^{2+} indicators (GECIs) provide a solution to problems found with injectable dyes but until recently have not been used in PCs (acutely, Badura et al. 2014; Kuhn et al. 2012; Najafi et al. 2014). The inability to maintain a clear window long enough to image, particularly after viral injections, could account for this scarcity. PCs, with elaborate dendritic arbors approaching the pial surface, may be highly amenable to damage during surgery, and problems creating a long-lasting window over the cerebellum (Nishiyama et al. 2014) contribute to this difficulty. Here we installed a stable cranial window over healthy cerebellar lobules crus I and II and tested GECIs expressed specifically in PCs. We chose crus I and II because multiple properties of PC

Address for reprint requests and other correspondence: J. M. Christie, Max Planck Florida Inst. for Neuroscience, 1 Max Planck Way, Jupiter, FL 33458 (e-mail: jason.christie@mpfi.org).

activity in crus I and II have been linked to licking behavior, including correlations with population complex spike rates (Welsh et al. 1995) and simple spike rates (Bryant et al. 2009; Hayar et al. 2006), which may regulate rhythmic licking frequency (Bryant et al. 2010). Imaging dendrites where widespread Ca^{2+} activity follows climbing fiber-driven complex spiking (Kitamura and Hausser 2011; Ozden et al. 2009; Schultz et al. 2009), we found that both GCaMP6f and R-CaMP2 enabled monitoring of activity in awake mice across many imaging sessions spread over many weeks. Several properties of this Ca^{2+} activity remained stable: event rates, the presumptive PC response area, and the spatial correlations of activity across cells in an imaging field. We investigated lick-related PC activity and identified a region of crus II that showed Ca^{2+} activity aligned with both the onset and timing of licking behavior. We then trained mice to lick in response to different sensory cues and observed increased, transient Ca^{2+} activity at the onset of cued rhythmic licking.

METHODS

Mice. All animal procedures were carried out with the approval of the Institute Animal Care and Use Committee at Max Planck Florida Institute (MPFI). Data were collected from 13 adult mice (10 female, 3 male; >10 wk of age at time of window installation surgery) including the following lines: B6;129S-Gt(ROSA)26Sortm38(CAG-GCaMP3)Hze/J (Jackson Labs stock no. 014538; Zariwala et al. 2012) and B6.129-Tg(Pcp2-cre)2Mpin/J (Jackson Labs stock no. 004146; Barski et al. 2000).

Surgical procedures. Before surgery (10–15 min), mice were injected with carprofen (5 mg/kg subcutaneous) and buprenorphine (0.35 mg/kg subcutaneous) for pain, dexamethasone (3 mg/kg subcutaneous) to reduce brain swelling, and D-mannitol (750 mg/kg intraperitoneal; Sigma) to enhance virus spread. A lidocaine-bupivacaine cocktail was used as a local anesthetic. All procedures were performed under isoflurane (1.5–2.0% by volume in O_2) to maintain a surgical plane of anesthesia as determined by nonresponsiveness to toe pinch. Eye ointment was applied under anesthesia at the start of surgery. Animals were held in a custom-built apparatus using ear bars to stabilize the head. Body temperature was set with a heating pad and controller using biofeedback from a rectal thermocouple.

For the surgical procedure, we first removed the skin above the skull and cleaned the opening of the periosteum and any membranous tissue. Once this was thoroughly dry, a thin layer of cyanoacrylate adhesive (Vetbond, 3M) was applied to the skull and then a custom-made stainless steel head post was cemented in place over the midline of the cortex with Metabond (Parkell). A cranial window was cut carefully with a scalpel (Chery et al. 2011) on the left side of the skull above the cerebellum centered on a region about 3.5 mm and 2.2 mm (lateral and caudal, respectively) from lambda. Care was taken not to damage the dura overlying the brain. The window was a small rectangle ~2 mm × 1.5 mm. After skull excision, an artificial cerebrospinal fluid solution (in mM: 142 NaCl, 5 KCl, 3.1 $CaCl_2$, 1.3 $MgCl_2$, 10 glucose, and 10 HEPES; all purchased from Sigma) was used to keep the brain moist and provide an interface to the window. The brain was covered with a small circular coverslip (64-0720, Warner Instruments) that was cemented into position with Metabond. Mice were carefully monitored during surgical recovery, with all animals showing normal behavior including the absence of motor deficits. Mice were allowed to recover at least 7 days before proceeding to imaging or water restriction.

Viral injections. With the exception of GCaMP3, GECIs were transduced in PCs with adeno-associated virus (AAV) (AAV1.CAG.Flex.GCaMP6f.WPRE.SV40 or AAV1.CAG.DIO.R-CAMP2.WPRE.SV40, both packaged at the University of Pennsylvania Vector Core Facility). For viral injections, we used beveled glass micropipettes to puncture the dura, inserting the tip ~200–250 μm deep into the brain to target the PC layer. Injections occurred before the glass coverslip was placed over the cranial opening. Injections were directed to three equally spaced locations near the edges of the cranial window (150–200 nl per location; perfusion rate of ~20 nl/min). After ejection of the viral solution, the pipette was held in place for 5 min before withdrawal.

Fluorescence imaging. For in vivo imaging, we used a custom-built laser-scanning microscope based on a MIMMS platform (D. Flickinger, Janelia Research Campus; https://openwiki.janelia.org/wiki/display/shareddesigns/MIMMS) with two-photon excitation (Chameleon Vision S, Coherent), a movable objective (MOM, Sutter Instruments), and an 8-kHz resonant scanner (CRS 8K, Cambridge Technologies) paired with a galvanometer mirror for beam steering. Hamamatsu photosensors (H10770PA-40) were used for nondescanned fluorescence detection with signal conditioning using preamplifiers (DHCPA-100, Femto). Computer-to-hardware interfacing was achieved with a PXIe-6341 DAQ and a PXIe-7961R FPGA module with a NI 5734 digitizer (National Instruments). Excitation wavelengths were 900 nm for GCaMPs and 1,020 nm for R-CaMP2. Emission was sent through a 570-nm dichroic, followed by a 525/70 filter for GCaMPs and a 630/75 filter for R-CaMP2. The laser power out of the objective was typically <30 mW for GCaMP6f and <60 mW for GCaMP3 and R-CaMP2. All imaging was performed with a ×16, 0.8 NA water dipping objective (Nikon). The objective was rotated to an angle that allowed the mouse to remain in a natural upright position during imaging. Ultrasound gel (Aquasonic Clear, Parker Laboratories, diluted ~1:10 with distilled water) was used as the immersion fluid to maintain a meniscus at extreme imaging angles. Images were collected with ScanImage 5 software (Vidrio Technologies) at 512 × 512 pixels with a 30 Hz frame rate. The resulting imaging field was ~330 μm per side. Course positioning, directed by the microscope stage coordinates, allowed for reimaging the same field of view across multiple sessions; fine alignment was achieved by using cellular landmarks during live imaging. In some cases we collected multiple imaging fields from a single animal.

The data in Fig. 1*A* were collected after first perfusing the animal with paraformaldehyde and then sectioning the cerebellum with a microtome. Images were collected on a Zeiss LSM 780 Axio Imager 2 using 488-nm excitation and 493- to 598-nm emission.

Behavior task. Mice were trained to perform licking tasks including a vibrissa-based object localization task with water rewards for motivation (O'Connor et al. 2010). Beginning at least 10 days prior to and then throughout training, mice were limited to 1 ml of water per day (food ad libitum). All mice on water restriction were monitored daily for health problems. Mice were housed in a reverse light-dark cycle room so that training and experiments could be performed during the dark cycle.

Mice were restrained in a custom-built closed-loop behavioral apparatus by head fixation. Mice rested comfortably in a metal tube with their head protruding from one end and their paws grasping the bottom edge of the tube. The apparatus was fully enclosed for light and noise restriction; mice were continuously monitored with infrared (940 nm) videography. A metal lickport was positioned immediately in front of the mouth (~2 mm) within reach of the tongue. Licks were reliably detected electronically (Slotnick 2009) when the tongue closed a circuit between the metal tube and the lickport. Precise water delivery was controlled with a solenoid valve (INKA2424212H, Lee) located outside of the behavioral apparatus. Tone cues were produced at 6 kHz with a custom-made sound board (Anidea Engineering). The stimulus objects were small-diameter (0.5 mm) steel poles (class ZZ pin gage 112100500, Vermont Gage). The positions of the poles were articulated in the lateral dimension with linear actuators (NA08B30-T4-MCO4, A-MCA-KT05, Zaber Technologies) and in the vertical dimension with pneumatic slides controlled by solenoid valves (SLS-10-30-P-A, CPE10-M1BH-5L-QS-6, Festo). The apparatus was controlled with an open-source software platform (BControl; C. Brody,

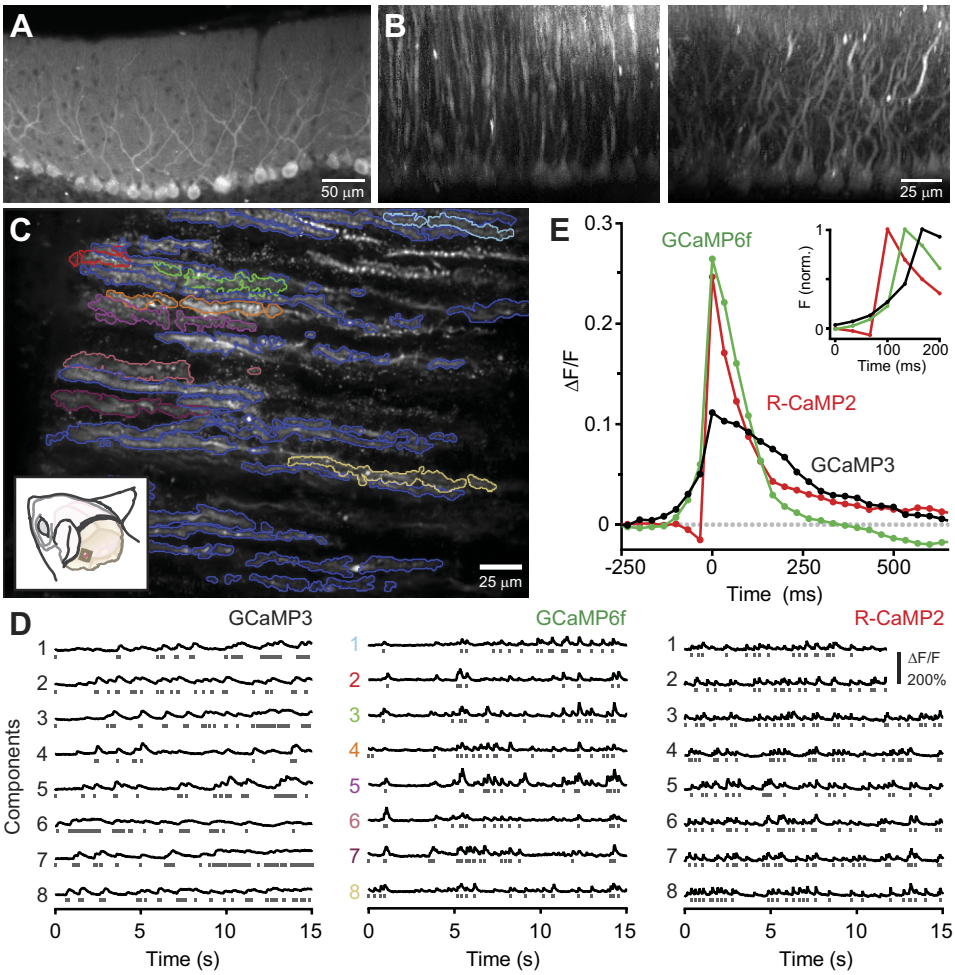

Fig. 1. Comparison of genetic Ca^{2+} indicators expressed in Purkinje cells (PCs). *A*: fixed tissue sagittal slice of GCaMP3-expressing PCs in GCaMP3 × Pcp2-cre mice. Note the absence of label in the molecular layer interneurons (dark spots among the labeled PC dendrites). *B*: coronal (*left*) and sagittal (*right*) reconstructions from a *z* stack of in vivo-imaged GCaMP3-expressing PCs. *C*: average intensity image of PC dendrites expressing GCaMP6f. Colored outlines indicate individual dendrites identified with spatial independent component analysis. *Inset*: approximate location of cranial window. *D*: Ca^{2+} fluorescence traces from individual components. Data are plotted as change in fluorescence divided by the baseline fluorescence (ΔF/F). Traces from 8 components are shown for each Ca^{2+} indicator: GCaMP3, GCaMP6f, and R-CaMP2. For GCaMP6f, the color-coded components correspond to the example average intensity image (dark blue components not illustrated in plot). Lines beneath each trace mark the locations of individual Ca^{2+} events. Observed differences in short-term Ca^{2+} event rates were likely related to changes in activity levels of the awake mice. *E*: fractional change in fluorescence plotted vs. time for isolated Ca^{2+} events. For this analysis, only isolated events were included (overlapping events occurring with 150 ms of the peak were rejected). The zero time point marks the peak fluorescence. *Inset*: events are shown aligned to onset (defined as last time point before data deviated >3 SDs from baseline). Data from multiple mice were included for each indicator (n = 292 events for GCaMP3, n > 10,000 events for GCaMP6f, and n = 3,418 events for R-CaMP2).

Princeton University; http://brodywiki.princeton.edu/bcontrol/index.php/Main_Page) ensuring precise timing. This was deployed on a RT Linux machine (JAF International) with a PCI-6025E DAQ board (National Instruments) for instrument input and output, communicating over Ethernet to a second computer running custom-written behavior routines (MATLAB, MathWorks). Outputs sent to solid-state relays controlled valve openings.

Data analysis. All image analysis was performed with custom routines in MATLAB. Time-series images were first aligned with a least-squares algorithm. Similar to previously published methods (Mukamel et al. 2009), identification of spatial filters corresponding to individual PC dendrites was accomplished with fast spatial independent component analysis (Hyvarinen 1999; http://research.ics.aalto.fi/ica/fastica/). Identified components were inspected post hoc, removing overlapping components and those that did not obviously correspond to dendrites (e.g., anomalous objects including PC somata that sometimes were inside the image field). Also, small components (<100 pixels) were automatically rejected from further analysis. Once these dendrite components were identified, we used the resulting binary masks for event analysis and to calculate component areas. Dendritic Ca^{2+} events were detected by an inference method (Vogelstein et al. 2010) with initialization parameters including a decay rate of 200 ms, a firing rate of 1 Hz, and a standard deviation of observation noise of 0.1. Our selection criteria included events three standard deviations above baseline; the resulting events were collected in a binary event matrix. Although our method was not free from error, it did appear to reach a level of accuracy similar to that reported by others (Mukamel et al. 2009; Ozden et al. 2008). Dendritic Ca^{2+} event probabilities were calculated by summing the number of events detected in each frame divided by the total number of dendrite components. Values for event rates and component sizes are presented in the text as means ± SE of imaging fields rather than for independent components. For comparison of the spatial correlations of PC Ca^{2+} events, the position of each dendrite was calculated by finding the centroid of the binary dendrite mask. The distance between two dendrites was then calculated as the distance between centroids. For spatial correlation the Pearson correlation coefficient was calculated as in Ozden et al. (2008). Lick probabilities were calculated by binning the lick detection times and dividing the number of licks in each bin by the total number of licks.

RESULTS

Testing GECIs in PCs. We developed chronic functional imaging in mouse cerebellum using a cranial window site over lobules crus I and II. These cerebellar regions are related to sensorimotor functions of the orofacial area including the tongue (Bryant et al. 2009, 2010; Welsh et al. 1995). Chronic imaging requires a stable, clear cranial window, a technique reported to be difficult in the mouse cerebellum (Nishiyama et al. 2014). We found that three factors could help improve our success rate. First, we typically used mice older than 70 days to reduce the rate of bone regrowth. Second, we cut the cranial window with a scalpel (Chery et al. 2011) as opposed to using a dental drill (Holtmaat et al. 2009). Cutting is less invasive than drilling, which, through vibration and heat, is more prone to damaging underlying brain tissue. Additionally, the cleaner

cut with the scalpel may help limit bone regrowth. Third, we placed the glass window directly on the skull, making slight contact with the brain surface, and only used a thin aqueous layer of artificial cerebrospinal fluid as an interface. This method produced sufficient pressure on the brain to reduce motion artifacts without causing clear signs of damage. In contrast, we found that additional pressure created by placing the coverslip inside the skull opening (Nishiyama et al. 2014) or by putting agarose between the coverslip and brain (Hoogland et al. 2015) caused damage to some PCs that became apparent over time (data not shown).

We next tested methods for expressing and imaging GECIs in PCs. Successful monitoring of Ca^{2+} activity requires several key demands: fast on and off binding rates so rapid events can be identified, strong fluorescence that simplifies automated cell identification and Ca^{2+} spike detection, and stable expression that persists over several weeks of experimentation. Mouse reporter lines are advantageous for this purpose because of the regulated, long-term expression of transgenes in well-defined cell populations (Madisen et al. 2010). We used a conditional GCaMP3 reporter mouse (Ai38) crossed with a Pcp2-cre line to specifically target expression in PCs (Zariwala et al. 2012), combined with resonant-scanning microscopy and two-photon excitation to collect high-frame rate fluorescence images from awake, head-restrained mice. In Pcp2-cre mice, visible GCaMP3 expression was limited to PCs (as observed in fixed tissue; Fig. 1*A*), and the cranial window allowed for imaging down to the PC somata in vivo (Fig. 1*B*). From our two-photon images, we used a spatial independent component algorithm (Hyvarinen 1999) to automatically group like-responding pixels belonging to components comprising individual PC dendrites (Mukamel et al. 2009). A typical result of cell sorting is shown in Fig. 1*C*. Next, we calculated fluorescence for each dendrite component (Fig. 1*D*). Finally, we used an inference algorithm (Vogelstein et al. 2010) to identify individual Ca^{2+} events (Fig. 1*D*). Ca^{2+} event detection is critical for understanding PC activity because Ca^{2+} levels in dendrites arise almost exclusively from the climbing fiber-driven complex spike (Kitamura and Hausser 2011; Ozden et al. 2009; Schultz et al. 2009). We found that although all PCs expressed GCaMP3, the relatively slow on and off rates and low signal-to-noise ratio (Chen et al. 2013) made it difficult to identify individual Ca^{2+} events (Fig. 1*D*). Consequently, GCaMP3 may be a poor choice for applications requiring rigorous quantification of Ca^{2+} events.

To overcome the limits of GCaMP3, we evaluated the faster indicators GCaMP6f (Chen et al. 2013) and R-CaMP2 (Inoue et al. 2015), using viral transduction (AAV) in Pcp2-cre mice to ensure high, selective expression in PCs. Both indicators provided good time resolution for event detection (Fig. 1*D*). Additionally, both indicators showed stronger fluorescence changes than GCaMP3 (Fig. 1*E*), facilitating dendrite component detection. The indicators had similar on rates ($\leq$60 ms for GCaMP6f; $\leq$30 ms for R-CaMP2), off rates ($\tau \sim$150 ms for GCaMP6f and R-CaMP2), and fluorescence changes (26.5% for GCaMP6f and 24.7% for R-CaMP2) and reported similar average Ca^{2+} event rates (1.3 Hz with GCaMP6f and 1.5 Hz with R-CaMP2). Thus both GCaMP6f and R-CaMP2 appear well-suited for quantitative reporting of PC activity. However, for the remainder of our experiments, we used GCaMP6f mainly because the laser power required for its two-photon excitation in PC cells at 900 nm was nearly twofold less than what was needed to excite R-CaMP2 at 1,020 nm, hence alleviating concern about photo-induced damage with extensive, repeated illumination.

Stability of PC Ca^{2+} activity over time. We imaged awake mice between 2 and 7 wk after surgery to assess for differences in overall Ca^{2+} activity with increasing time from window installation. We used 2 wk as a starting point to allow for onset of gene expression and for the brain to recover from surgery (Holtmaat et al. 2009). Beyond 7 wk the number of GECI-expressing PCs diminished, as has been reported previously (Kuhn et al. 2012). We found that dendritic Ca^{2+} event rates fell mostly within the 1–2 Hz range (mean for imaging fields = 1.34 $\pm$ 0.04 Hz; Fig. 2*A*), as previously reported for PCs in awake, active mice (Ghosh et al. 2011; Mukamel et al. 2009; Ozden et al. 2012). In grouped data across animals, we observed no clear trend in event rates against postsurgery observation time (R^2 = 0.016). We also examined the size of the presumptive dendrites by calculating the mean area of individual dendritic components in an imaging field (Fig. 2*B*). In grouped data, the average size of these components was similar (overall mean = 130.6 $\pm$ 3.0 μm^2) and not related to imaging time point (R^2 = 0.009). Similar results were also obtained with R-CaMP2 (Fig. 2). Taken together, the regularity of firing

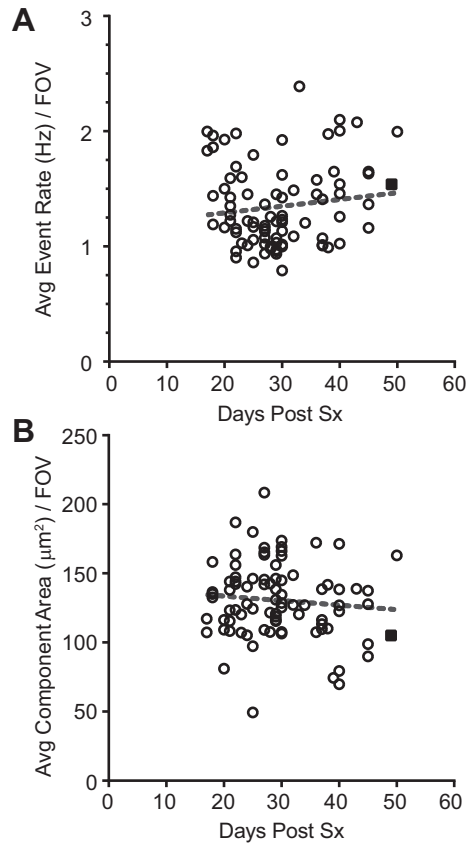

Fig. 2. Ca^{2+} imaging parameters remain stable for weeks after window implantation. Event rate (*A*) or area (*B*) of identified independent components is plotted vs. days after cranial window and virus injection surgery. Each circle represents an average measurement of all components (range = 8–48 components) in a single imaging field labeled with GCaMP6f (n = 85 imaging fields from 10 mice). Linear trends are shown as dashed gray lines. Filled square data point at 49 days is from PCs labeled with R-CaMP2, demonstrating the similar stability of this indicator. FOV, field of view.

rates and dendritic area indicate that the PCs remained healthy and our window remained clear over prolonged periods.

The key advantage of chronic imaging lies in the opportunity to repeatedly observe the same cells during behavioral learning periods. Therefore, we next imaged the same cerebellar regions over multiple imaging sessions each separated by at least 1 day (mean 4.5 days; range 2–15 days). On examination, we could repeatedly identify the same groups of cells within the same imaging field as apparent in the similar shapes of dendrite components (Fig. 3*A*). Overall we tracked 19 imaging fields across multiple days and found that the average size of components remained relatively stable throughout four imaging sessions (122.1 ± 4.9 μm^2 and 125.9 ± 11.1 μm^2, first and fourth sessions, respectively; Fig. 3, *B* and *C*). To test the stability of the activity in these areas, we compared dendritic Ca^{2+} event rates across imaging sessions (Fig. 3, *D* and *E*). Overall, mean event rates were relatively stable (1.3 Hz). Moreover, average event rates were similar whether we used the dendrite components identified in each session or reused the masks from the first session (Fig. 3*D*). The trial-to-trial differences in event rates are likely due to the relationship between complex spike rates and overall motor activity (Ghosh et al. 2011; Mukamel et al. 2009).

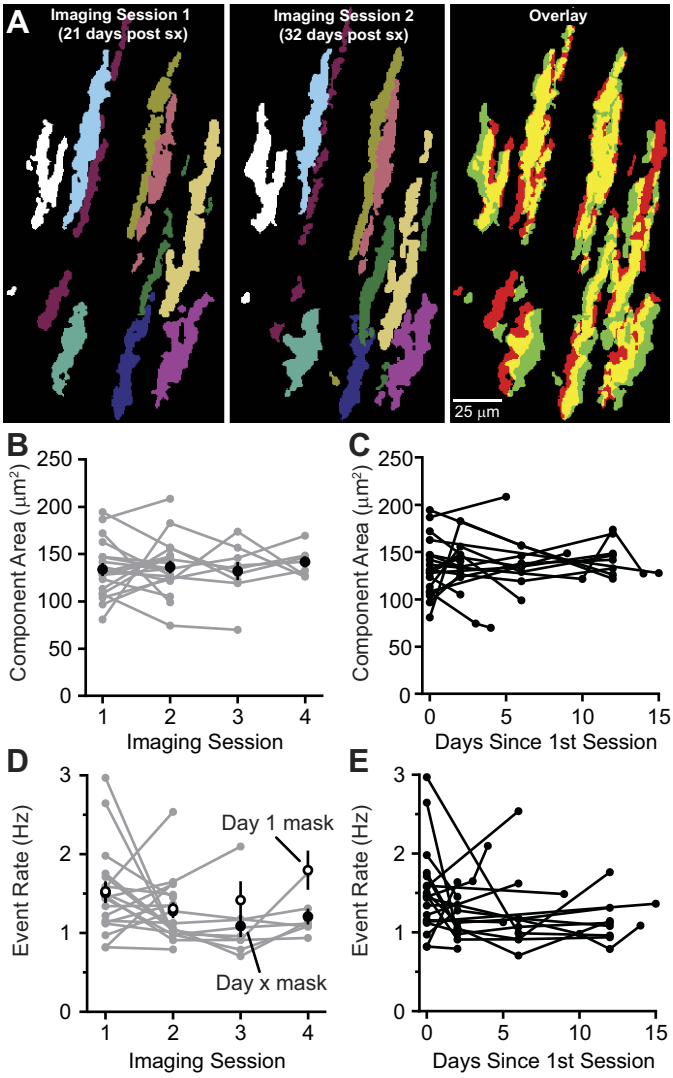

Fig. 3. Dendrite components can be repeatedly imaged over several days. *A*: representative images showing 10 components identified either 21 (*left*) or 32 (*center*) days after window installation. Matching colors indicate matching components. For clarity, not all identified components are shown. *Right*: overlay of *left* (red) and *center* (green) images. *B*: component area plotted vs. successive imaging day (which were typically not consecutive days). Connected gray traces indicate data from individual imaging fields. Filled circles show the average. Error bars represent SE. *C*: same data as *B* with data plotted vs. days since the region was first imaged. *D*: event rate plotted vs. imaging day. Connected gray traces indicate data from individual imaging fields where independent dendrite components were identified on each imaging day. Filled circles show the average of these data (*day x* mask). Open circles show the average when rates were calculated with the independent dendrite components identified on imaging *day 1* (*day 1* mask). Error bars represent SE. *E*: as in *C* except for event rate. Data in *B–E* collected from 19 imaging fields in 8 mice.

Complex spikes occur synchronously in sagittal bands of PCs, with concerted activity between any two PCs within an ensemble inversely proportional to their mediolateral separation. Coherence of Ca^{2+} activity is particularly strong in active mice (De Gruijl et al. 2014; Hoogland et al. 2015; Mukamel et al. 2009; Ozden et al. 2012; Schultz et al. 2009; Tsutsumi et al. 2015). We asked whether this property also remained stable over time. We first measured the distance between pairs of functionally identified dendrites and then calculated the correlation of their respective fluorescence. As previously reported, Ca^{2+} activity in nearby PC dendrites showed a greater level of correlation than for more spatially separated dendrites (Fig. 4*A*). We observed nearly identical results when we repeated this analysis on data collected at least 2 days later (mean 4.4 days), using the same dendrite component masks from the first imaging session (Fig. 4*B*). In summary, these data establish that the activity in individually identified PC dendrites can be repeatedly assessed across multiple imaging sessions, over time, without causing gross changes to their activity.

PC activity in response to trained licking behavior. Cerebellar lobule crus II is known to integrate sensorimotor aspects of licking including tongue-related movements during the consumption of water (Bryant et al. 2009, 2010; Welsh et al. 1995). Thus we chose to examine PCs in this region for dendritic Ca^{2+} activity related to licking. Mice were water-restricted to strongly motivate licking behavior. This involved several days of limited water intake (≥10 days) that began only after the mouse had recovered from surgery (>5 days). Water-restricted mice were acclimated to head restraint over a period of several days and were trained to consume small aliquots (~4 μl) of water from a lickport (Guo et al. 2014; O'Connor et al. 2010). After lickport training, we imaged PC activity during bouts of licking induced when water was dispensed at regular intervals from the port (0.5 Hz). During each bout, mice licked rhythmically (~6 Hz). Correspondingly, dendritic Ca^{2+} event probability varied with lick rate (Fig. 5*A*), similar to previous electrical recording results (Welsh et al. 1995) and also to those obtained with simple spike firing (Bryant et al. 2009, 2010). We more carefully explored the temporal and spatial representation of PC activity during bouts of licking and found regional differences in crus II. In one region, we observed a particularly sharp increase in dendritic Ca^{2+} events on each trial when water became available (Fig. 5, *B* and *C*). In other regions, not only was this response not apparent but the Ca^{2+} event correlation to lick rate was much weaker and out of phase compared with the responsive region (Fig. 5, *A–C*). Together, these results led us to speculate that this responsive subregion of crus II could be related to the initiation of motor action associated with licking. In support of this idea,

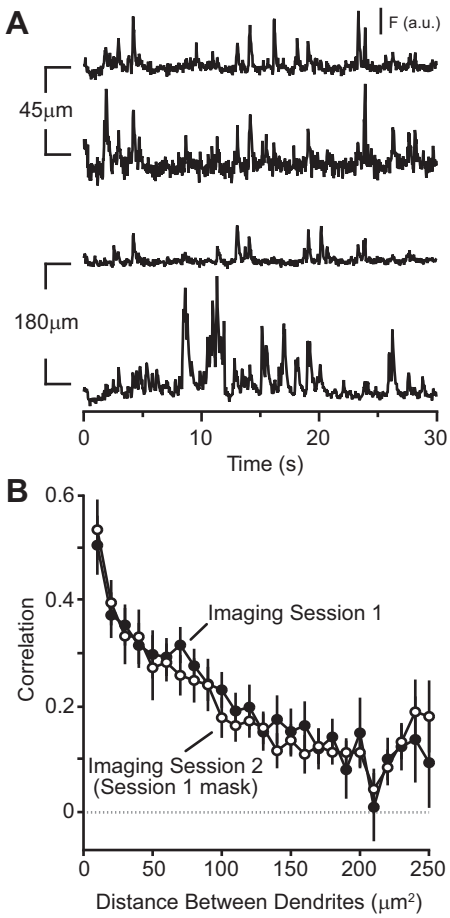

Fig. 4. Spatial correlation of Ca^{2+} activity is stable across days. *A*: raw fluorescence traces from individual dendrite components. *Top* 2 dendrites were separated by 45 μm, and *bottom* 2 dendrites were separated by 180 μm. *B*: plot of the pairwise correlation coefficient vs. the distance between the centroids of each dendrite pair. Filled circles show average of data collected on the first day of imaging. Open circles show average of data collected on the second day of imaging but analyzed with the independent dendrite components identified on *day 1* (*session 1* mask). Data collected from 17 image fields in 8 mice. Error bars indicate SE.

Ca^{2+} event probability remained unchanged in the cases when the water valve opened but the mouse did not lick (Fig. 5*B*), and Ca^{2+} activity closely preceded the onset of licking following water delivery (Fig. 5*D*).

Building on this observation, we next trained these mice to lick in response to cues. First, mice were taught a simple association task in which the availability of water was indicated by an audible tone. Mice quickly learned to adapt their behavior accordingly by generally withholding licking until the tone sounded and then licking for several seconds until the water droplet was consumed (Fig. 6*A*). Similar to our previous result, we observed a sharp increase in PC dendritic Ca^{2+} events that were time-locked to tone onset in the lick-responsive region of crus II (Fig. 6*B*). PCs in this region were not responsive to the tone cue in untrained mice (data not shown). To provide a separate cue for licking behavior, we trained another set of mice to perform a vibrissa-based object localization task in which vibrissa contact with a pole located in a preferred "Go" position is associated with a water reward (O'Connor et al. 2010). After at least 8 days of training, mice learned to distinguish the preferred position from a distractor "No-Go" location by withholding licking to avoid a short time-out punishment (Fig. 6*C*). Well-trained mice licked reliably on Go trials (>80% correct; Fig. 6*D*), with the behavioral onset of licking within a well-timed window during the reward period (Fig. 6*D*). The solenoids that control the pole movements may provide an additional audible cue for the mice to initiate licking behavior. However, after whisker removal, mice performed at chance levels (Fig. 6*E*), indicating that the licking cue was vibrissa based.

In the lick-responsive region of crus II, we observed an increase in dendritic Ca^{2+} event probability in PCs during Go trials (Fig. 6*F*), with the highest likelihood occurring immediately prior to the initiation of licking. PC activity was indistinguishable from baseline levels during No-Go trials when mice refrained from licking. The amplitude of the dendrite event probability in the Go trials increased as the timing of licking improved with training (Fig. 6*G*; *session 1* and *session 2* were separated by a training session without PC imaging). These data confirm that a subregion of crus II has increased PC Ca^{2+} activity prior to the onset of licking.

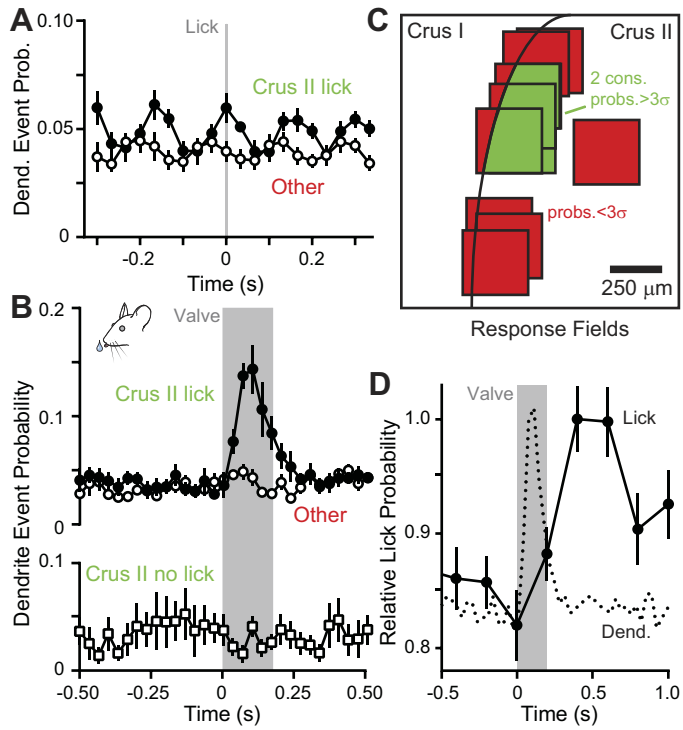

Fig. 5. Identification of a lick-related region of crus II. *A*: peristimulus time histogram of dendrite event probability aligned to tongue contact with the lick detector (gray line). Data were collected from lick-responsive (green) and nonresponsive (red) regions of crus II (n = 10 and 12 imaging fields, respectively; 3 mice). *B*, *top*: summary plot showing PC dendrite Ca^{2+} event probability aligned to water availability lick-responsive and nonresponsive areas (n = 10 and 12 imaging fields, respectively; 3 mice). The water valve open time is depicted as a gray bar. *Bottom*: event probability in the crus II lick-responsive region when the water valve opened but the mouse did not lick (n = 8 imaging fields, 3 mice). *C*: cartoon map depicting imaging subregions of crus II approximated using stage coordinates. Green areas indicate a region where the total population of identified PC dendrite components showed an increase in event probability of 3 SDs (σ) above the baseline level for 2 consecutive time points during the water availability, and red areas indicate areas that showed no significant response. *D*: lick detection probability plotted vs. time. Shown superimposed is the dendritic event probability of PCs in the crus II lick-responsive subregion. The gray bar indicates when the water valve was open. For all panels, data are presented as means ± SE.

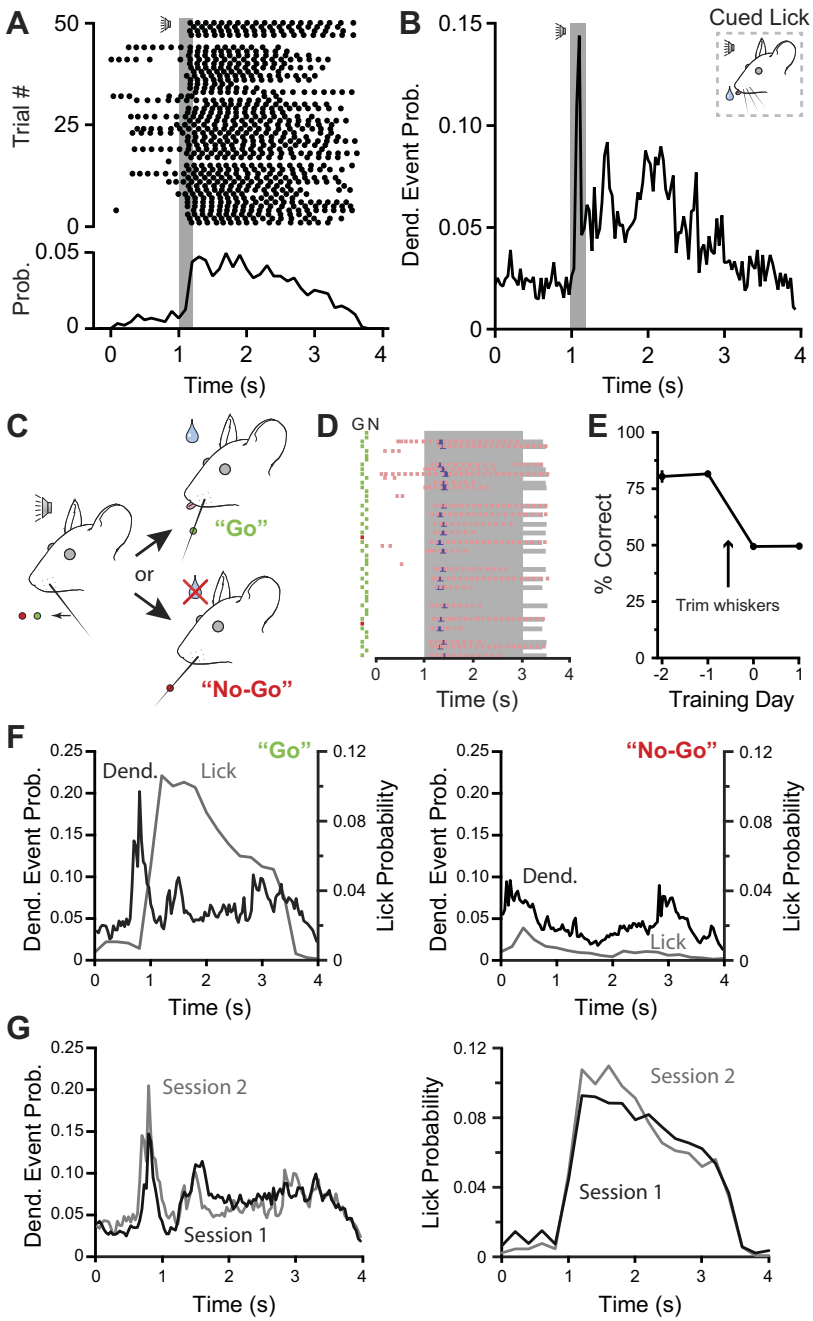

Fig. 6. Two behavioral tasks confirm lick dependence of dendritic Ca^{2+} events in crus II. *A*: mice were trained to lick in response to a tone cue. *Top*: example of the timing of licks detected during a series of 50 behavioral trials. Gray bar indicates timing of the tone. Dots are each detected lick. *Bottom*: lick probability summary of *top* panel. Licking increased ~6-fold with the sound cue. *B*: PC activity during tone-cued licking behavior. Dendrite Ca^{2+} event probability is plotted vs. time. The timing of the tone cue is indicated by the gray bar. *C*: cartoon illustrating the pole discrimination task. *Left*: the mouse hears a tone and has to determine whether a pole is in the preferred "Go" or distractor "No-Go" location. *Top*: when the pole is in the Go location, the mouse licks to retrieve a water reward. *Bottom*: when the pole is in the No-Go location, the mouse refrains from licking to avoid a time-out. *D*: summary of 50 pole discrimination trials. Trial type [Go (G) or No-Go (N)] is plotted on *left*. Green trials were correct and red trials incorrect. Gray area indicates when the pole was in position. Water delivery time points are blue, and time points of detected licks are pink. *E*: plot showing that pole discrimination success rate changes after whisker trimming. Training day is plotted on the *x*-axis, with *day 0* occurring the day after whisker trimming. Mice dropped from >80% correct to chance levels. Data are presented as means ± SE ($n = 4$ mice). *F*: representative plots showing probability of dendrite Ca^{2+} events (black lines) and licking (gray lines) over time during the pole localization task. *Left*: Go trials where licking was present. *Right*: No-Go trials where minimal licking occurred. Data represent an average of 2 behavioral sessions of at least 200 trials. Similar results were observed in 2 other animals. *G*: Go data from *F*, but with traces from each imaging session plotted individually. Dendrite data (*left*) are plotted separately from lick data (*right*).

DISCUSSION

Converging advances in fluorescence microscopy, genetics, and behavior have led to unprecedented access to neuron-level experimentation in awake mice. Together, these techniques have been used to study many areas of the mouse brain, linking cell type-specific physiology to high-order function, but implementation in some regions has proven more difficult than in others. For example, even though the cerebellum, as a learning machine (Ito 2006), is ideally suited for in vivo analysis of neural circuits underlying dynamic behavior, the combinatorial use of all three techniques has been limited in its study. One reason is the difficulty in creating a high-quality cranial window amenable to chronic functional imaging. To date, only morphological studies have been reported in chronically imaged cerebellum (Allegra Mascaro et al. 2013; Carrillo et al. 2013a, 2013b; Kuhn et al. 2012). Even in cases where acute imaging of a GECI was performed, functional imaging occurred within 14 days of surgery (Badura et al. 2014; Kuhn et al. 2012; Najafi et al. 2014). In this report, we chronically imaged Ca^{2+} activity in PCs for up to 7 wk. This duration should be sufficient, as shown in experiments here, to functionally examine the cerebellum's involvement in complex motor tasks including volitional movements that require extensive training times or to resolve circuit changes accompanying perturbation.

Ca^{2+} imaging in the cerebellum. In the cerebellum, visualizing neuronal activity with two-photon microscopy has advantages over electrical recordings. For example, associative parallel fiber LTD depends largely on Ca^{2+} signaling in PC dendrites (reviewed in Finch et al. 2012). By imaging Ca^{2+} in

these structures, instead of electrical activity at the soma by electrodes, the biochemical pathway underlying this type of plasticity can be directly assessed. Our approach is ideally suited to track climbing fiber-induced Ca^{2+} changes in PCs and would therefore be amenable to observing alteration in the dendritic activity following climbing fiber LTD (Hansel and Linden 2000) or plasticity in the inferior olive (which may alter climbing fiber spiking patterns; Mathy et al. 2009, 2014). However, if any additional LTD occurs independent of the complex spike signal, then alternative approaches such as electrical recordings would be better suited. Ca^{2+} imaging also allows for dense sampling of activity in large cell populations at both cellular and subcellular resolution. In our experiments, we could reliably monitor tens of distinct PC dendrites in a single imaging field and record from $\sim$3 mm^2 of crus I and II in a single imaging session by repositioning the microscope. Thus we could build detailed response maps for cued behaviors such as licking. Building such a map with multiunit electrode recordings would have been difficult because of the large amount of averaging that is necessary to correlate complex spike activity to licking behavior (Bryant et al. 2010). Although we did not examine Ca^{2+} activity within individual dendrites in detail (in part because of the necessity of a sparse labeling method for such a study), subcellular imaging could potentially lead to further insight into climbing fiber-mediated plasticity. For example, while complex spikes are generally viewed as dendritewide cellular events (Kitamura and Hausser 2011; Ozden et al. 2009; Schultz et al. 2009), coincident stimulation of parallel fibers or interneurons with climbing fiber activation in acute cerebellar slices can increase Ca^{2+} levels in subsections of PC dendrites (Callaway et al. 1995; Finch et al. 2012; Wang et al. 2000), perhaps leading to partitioned plasticity. Climbing fiber-driven LTD is just one aspect of cerebellar physiology that is well-suited for study with our technique. However, one major limitation of all Ca^{2+} imaging methods in PCs is the inability to record simple spike activity because of high spike rates (e.g., $>$30 Hz) and minimal back-propagation of simple spikes into dendrites (Kitamura and Hausser 2011; Schultz et al. 2009). Moreover, electrical recordings also have temporal advantages over fluorescent indicators. While previous reports performed in vivo show that low-frequency complex spiking in PCs is accurately reported by two-photon Ca^{2+} imaging (Kitamura and Hausser 2011; Ozden et al. 2009; Schultz et al. 2009), experimental conditions where bursts of complex spikes occur (for example, Lang et al. 1996), electrical recordings might be better suited.

An incredible array of Ca^{2+} indicators exist, including both organic and genetically encoded variants. In the cerebellum, the cell-permeant Ca^{2+} indicator OGB-1/AM has been used extensively to study PC activity. While OGB-1/AM has worked well in acute experiments (De Gruijl et al. 2014; Hoogland et al. 2015; Mukamel et al. 2009; Najafi et al. 2014; Ozden et al. 2008, 2009, 2012; Schultz et al. 2009; Sullivan et al. 2005; Tsutsumi et al. 2015), the indicator has several drawbacks that limit its usefulness when more complex manipulations are required. OGB-1/AM is bolus loaded into the cerebellum, causing nonspecific labeling of other cell types (Nimmerjahn et al. 2009; Sullivan et al. 2005). The dye degrades over time, and therefore must be reinjected to persistently image activity. Given this short time window, imaging must occur within hours of when the brain was exposed for injection (Stosiek et al. 2003). Concerns about health of recently uncovered brain tissue (and electrode insertion) may cloud interpretation of results. We used a genetic approach that overcame many of these drawbacks.

We found that two fast GECIs, GCaMP6f and R-CaMP2 (with binding kinetics equal to or better than to OGB-1/AM; Chen et al. 2013; Inoue et al. 2015), robustly reported PC dendritic Ca^{2+} events with excellent resolution. Both were virally transduced using a Cre-dependent construct in a transgenic line specific for PC expression (as an alternative to Najafi et al. 2014, who used a dual viral injection, GCaMP6f and Cre) ensuring cell type specificity and long-term stability. Notably, we found the response properties of the red GECI R-CaMP2 to be quite comparable to the green GECI GCaMP6f, at least in PCs. In fact, the rapid binding rate and low Hill coefficient of R-CaMP2 (Inoue et al. 2015) may be advantageous for some experiments. In combined use, these spectrally separable chromophores may allow for simultaneous pre- and postsynaptic imaging (e.g., climbing fiber and PC) or combinatorial use with optogenetic effectors of activity (Inoue et al. 2015; Packer et al. 2015).

We started water restriction, behavioral manipulations, and Ca^{2+} imaging in PCs only after mice had several days to completely recover from surgery and anesthesia. For some behavioral manipulations, training involved multiple, time-involved steps that would be difficult to complete with an acute imaging approach. Therefore, a stable window allowing for chronic functional imaging enabled a new set of experimental procedures that would otherwise prove difficult. However, we imagine that the real benefit from this technique will be the ability to repeatedly survey cellular activity in the same areas during cerebellum-dependent learning or after imposition of a perturbation to disrupt circuit activity.

Relating behavior to cerebellar PC activity. In the cerebellum, sagittal bands of closely apposed PCs show coherent activity as represented in the Ca^{2+} changes in their dendrites (De Gruijl et al. 2014; Ozden et al. 2009). This coherence may be driven, in part, by coincident firing of similarly projecting climbing fibers mediated by gap junctional coupling in the inferior olive (De Gruijl et al. 2014; Schultz et al. 2009). Additional spatial organization may occur via climbing fiber-driven activation of molecular layer interneurons (Coddington et al. 2013; Mathews et al. 2012). While the mechanism is well studied, the importance of spatially and temporally coherent PC activity in vivo is not clear. By having a tool that can track PC activity over prolonged periods of time, we can explore whether correlated Ca^{2+} signaling is plastic. For example, the spatial and temporal aspects of coherence may be remodeled during learning, or disruption of this organization may affect behavior. We observed that the spatial coherence of PC dendrite activity was quite consistent; however, these were in relatively static conditions. Further investigation is required to establish whether learning or perturbation affects stability.

Increasingly, researchers are developing ever more sophisticated behavioral tasks to study the cognitive, sensory, and motor systems of mice. Most tasks are limited to conditions in which the animal must be head restrained to facilitate two-photon imaging, as we have done here. Still, these complex behaviors create many avenues for understanding how the dynamic responses of individual neurons within interconnected circuits function during these tasks. We focused on licking as

a behavioral output and identified a region of cerebellar crus II where PC activity was related to the consumption of water. The strong temporal relationship with lick rate suggests that this activity was linked to the timing and execution of rhythmic licking, perhaps because of motor-related function since the signal appeared in response to several different sensory cues. A motor rather than sensory function matches a finding in rats where cutting the trigeminal nerve had no effect on lick-related movements (Welsh et al. 1995). This interpretation is also consistent with the increased PC activity reported at the initiation of locomotion (Hoogland et al. 2015). Furthermore, we found slight differences in the representation of PC dendritic Ca^{2+} events as the mice gained experience with the task. We took this result to signify that the timing of the licking decision became more regular, in agreement with a study showing that activity arising from the inferior olive is required for proper cued lick timing (Welsh 1998). However, the importance of these signals as it relates to behavior or learning the task is not clear and may not relate to learning the pole discrimination task at all. However, it is possible that these signals help enforce proper timing of the task, including reward licking (Rahmati et al. 2014). Moving forward, combining the ability to chronically image Ca^{2+} with optogenetic control of the inferior olive should allow for both disruption of the lick-based Ca^{2+} events and monitoring of the resulting behavior.

ACKNOWLEDGMENTS

We thank Yishai Elyada (Hebrew University, Jerusalem) for advice on cranial windows and in vivo imaging, Luciana Walendy (Janelia Research Campus/MPFI) for advice on animal training, Randy Altshuler (MPFI) for lab support, the MPFI Animal Resource Center for animal husbandry and health monitoring, the MPFI Mechanical Workshop for design and fabrication assistance, the MPFI Molecular Core for plasmid DNA preparation, and the GENIE Program and the Janelia Research Campus including Vivek Jayaraman, Rex Kerr, Douglas Kim, Loren Looger, and Karel Svoboda for use of GCaMP6f.

GRANTS

This work was supported by the Max Planck Society, the MPFI for Neuroscience (J. M. Christie), and grants from AMED-CREST, Brain/MINDS from MEXT and AMED, and the Takeda Science Foundation (H. Bito).

DISCLOSURES

No conflicts of interest, financial or otherwise, are declared by the author(s).

AUTHOR CONTRIBUTIONS

Author contributions: M.A.G., S.B.A., and J.M.C. conception and design of research; M.A.G. and S.B.A. performed experiments; M.A.G. analyzed data; M.A.G., S.B.A., and J.M.C. interpreted results of experiments; M.A.G. and J.M.C. prepared figures; M.A.G. and J.M.C. drafted manuscript; M.A.G., S.B.A., H.B., and J.M.C. edited and revised manuscript; M.A.G., S.B.A., H.B., and J.M.C. approved final version of manuscript.

REFERENCES

Albus JS. A theory of cerebellar function. *Math Biosci* 10: 25–61, 1971.

Allegra Mascaro AL, Cesare P, Sacconi L, Grasselli G, Mandolesi G, Maco B, Knott GW, Huang L, De Paola V, Strata P, Pavone FS. In vivo single branch axotomy induces GAP-43-dependent sprouting and synaptic remodeling in cerebellar cortex. *Proc Natl Acad Sci USA* 110: 10824–10829, 2013.

Badura A, Sun XR, Giovannucci A, Lynch LA, Wang SS. Fast calcium sensor proteins for monitoring neural activity. *Neurophotonics* 1: 025008, 2014.

Barski JJ, Dethleffsen K, Meyer M. Cre recombinase expression in cerebellar Purkinje cells. *Genesis* 28: 93–98, 2000.

Bryant JL, Boughter JD, Gong S, LeDoux MS, Heck DH. Cerebellar cortical output encodes temporal aspects of rhythmic licking movements and is necessary for normal licking frequency. *Eur J Neurosci* 32: 41–52, 2010.

Bryant JL, Roy S, Heck DH. A technique for stereotaxic recordings of neuronal activity in awake, head-restrained mice. *J Neurosci Methods* 178: 75–79, 2009.

Burguiere E, Arleo A, Hojjati M, Elgersma Y, De Zeeuw CI, Berthoz A, Rondi-Reig L. Spatial navigation impairment in mice lacking cerebellar LTD: a motor adaptation deficit? *Nat Neurosci* 8: 1292–1294, 2005.

Callaway JC, Lasser-Ross N, Ross WN. IPSPs strongly inhibit climbing fiber-activated $[Ca^{2+}]_i$ increases in the dendrites of cerebellar Purkinje neurons. *J Neurosci* 15: 2777–2787, 1995.

Carrillo J, Cheng SY, Ko KW, Jones TA, Nishiyama H. The long-term structural plasticity of cerebellar parallel fiber axons and its modulation by motor learning. *J Neurosci* 33: 8301–8307, 2013a.

Carrillo J, Nishiyama N, Nishiyama H. Dendritic translocation establishes the winner in cerebellar climbing fiber synapse elimination. *J Neurosci* 33: 7641–7653, 2013b.

Chen TW, Wardill TJ, Sun Y, Pulver SR, Renninger SL, Baohan A, Schreiter ER, Kerr RA, Orger MB, Jayaraman V, Looger LL, Svoboda K, Kim DS. Ultrasensitive fluorescent proteins for imaging neuronal activity. *Nature* 499: 295–300, 2013.

Chery R, L'Heureux B, Bendahmane M, Renaud R, Martin C, Pain F, Gurden H. Imaging odor-evoked activities in the mouse olfactory bulb using optical reflectance and autofluorescence signals. *J Vis Exp* 56: e3336, 2011.

Coddington LT, Rudolph S, Vande Lune P, Overstreet-Wadiche L, Wadiche JI. Spillover-mediated feedforward inhibition functionally segregates interneuron activity. *Neuron* 78: 1050–1062, 2013.

De Gruijl JR, Hoogland TM, De Zeeuw CI. Behavioral correlates of complex spike synchrony in cerebellar microzones. *J Neurosci* 34: 8937–8947, 2014.

Finch EA, Tanaka K, Augustine GJ. Calcium as a trigger for cerebellar long-term synaptic depression. *Cerebellum* 11: 706–717, 2012.

Ghosh KK, Burns LD, Cocker ED, Nimmerjahn A, Ziv Y, Gamal AE, Schnitzer MJ. Miniaturized integration of a fluorescence microscope. *Nat Methods* 8: 871–878, 2011.

Guo ZV, Hires SA, Li N, O'Connor DH, Komiyama T, Ophir E, Huber D, Bonardi C, Morandell K, Gutnisky D, Peron S, Xu NL, Cox J, Svoboda K. Procedures for behavioral experiments in head-fixed mice. *PLoS One* 9: e88678, 2014.

Hansel C, Linden DJ. Long-term depression of the cerebellar climbing fiber-Purkinje neuron synapse. *Neuron* 26: 473–482, 2000.

Hayar A, Bryant JL, Boughter JD, Heck DH. A low-cost solution to measure mouse licking in an electrophysiological setup with a standard analog-to-digital converter. *J Neurosci Methods* 153: 203–207, 2006.

Holtmaat A, Bonhoeffer T, Chow DK, Chuckowree J, De Paola V, Hofer SB, Hubener M, Keck T, Knott G, Lee WC, Mostany R, Mrsic-Flogel TD, Nedivi E, Portera-Cailliau C, Svoboda K, Trachtenberg JT, Wilbrecht L. Long-term, high-resolution imaging in the mouse neocortex through a chronic cranial window. *Nat Protoc* 4: 1128–1144, 2009.

Hoogland TM, De Gruijl JR, Witter L, Canto CB, De Zeeuw CI. Role of synchronous activation of cerebellar Purkinje cell ensembles in multi-joint movement control. *Curr Biol* 25: 1157–1165, 2015.

Hyvarinen A. Fast and robust fixed-point algorithms for independent component analysis. *IEEE Trans Neural Netw* 10: 626–634, 1999.

Inoue M, Takeuchi A, Horigane S, Ohkura M, Gengyo-Ando K, Fujii H, Kamijo S, Takemoto-Kimura S, Kano M, Nakai J, Kitamura K, Bito H. Rational design of a high-affinity, fast, red calcium indicator R-CaMP2. *Nat Methods* 12: 64–70, 2015.

Ito M. Cerebellar circuitry as a neuronal machine. *Prog Neurobiol* 78: 272–303, 2006.

Ito M, Sakurai M, Tongroach P. Climbing fibre induced depression of both mossy fibre responsiveness and glutamate sensitivity of cerebellar Purkinje cells. *J Physiol* 324: 113–134, 1982.

Jacobson GA, Rokni D, Yarom Y. A model of the olivo-cerebellar system as a temporal pattern generator. *Trends Neurosci* 31: 617–625, 2008.

Ke MC, Guo CC, Raymond JL. Elimination of climbing fiber instructive signals during motor learning. *Nat Neurosci* 12: 1171–1179, 2009.

Kimpo RR, Rinaldi JM, Kim CK, Payne HL, Raymond JL. Gating of neural error signals during motor learning. *Elife* 3: e02076, 2014.

Kitamura K, Hausser M. Dendritic calcium signaling triggered by spontaneous and sensory-evoked climbing fiber input to cerebellar Purkinje cells in vivo. *J Neurosci* 31: 10847–10858, 2011.

Koekkoek SK, Hulscher HC, Dortland BR, Hensbroek RA, Elgersma Y, Ruigrok TJ, De Zeeuw CI. Cerebellar LTD and learning-dependent timing of conditioned eyelid responses. *Science* 301: 1736–1739, 2003.

Kuhn B, Ozden I, Lampi Y, Hasan MT, Wang SS. An amplified promoter system for targeted expression of calcium indicator proteins in the cerebellar cortex. *Front Neural Circuits* 6: 49, 2012.

Lang EJ, Sugihara I, Llinas R. GABAergic modulation of complex spike activity by the cerebellar nucleoolivary pathway in rat. *J Neurophysiol* 76: 255–275, 1996.

Ly R, Bouvier G, Schonewille M, Arabo A, Rondi-Reig L, Lena C, Casado M, De Zeeuw CI, Feltz A. T-type channel blockade impairs long-term potentiation at the parallel fiber-Purkinje cell synapse and cerebellar learning. *Proc Natl Acad Sci USA* 110: 20302–20307, 2013.

Madisen L, Zwingman TA, Sunkin SM, Oh SW, Zariwala HA, Gu H, Ng LL, Palmiter RD, Hawrylycz MJ, Jones AR, Lein ES, Zeng H. A robust and high-throughput Cre reporting and characterization system for the whole mouse brain. *Nat Neurosci* 13: 133–140, 2010.

Marr D. A theory of cerebellar cortex. *J Physiol* 202: 437–470, 1969.

Mathews PJ, Lee KH, Peng Z, Houser CR, Otis TS. Effects of climbing fiber driven inhibition on Purkinje neuron spiking. *J Neurosci* 32: 17988–17997, 2012.

Mathy A, Clark BA, Hausser M. Synaptically induced long-term modulation of electrical coupling in the inferior olive. *Neuron* 81: 1290–1296, 2014.

Mathy A, Ho SS, Davie JT, Duguid IC, Clark BA, Hausser M. Encoding of oscillations by axonal bursts in inferior olive neurons. *Neuron* 62: 388–399, 2009.

Medina JF, Lisberger SG. Links from complex spikes to local plasticity and motor learning in the cerebellum of awake-behaving monkeys. *Nat Neurosci* 11: 1185–1192, 2008.

Mukamel EA, Nimmerjahn A, Schnitzer MJ. Automated analysis of cellular signals from large-scale calcium imaging data. *Neuron* 63: 747–760, 2009.

Najafi F, Giovannucci A, Wang SS, Medina JF. Sensory-driven enhancement of calcium signals in individual Purkinje cell dendrites of awake mice. *Cell Rep* 6: 792–798, 2014.

Nimmerjahn A, Mukamel EA, Schnitzer MJ. Motor behavior activates Bergmann glial networks. *Neuron* 62: 400–412, 2009.

Nishiyama N, Colonna J, Shen E, Carrillo J, Nishiyama H. Long-term in vivo time-lapse imaging of synapse development and plasticity in the cerebellum. *J Neurophysiol* 111: 208–216, 2014.

O'Connor DH, Clack NG, Huber D, Komiyama T, Myers EW, Svoboda K. Vibrissa-based object localization in head-fixed mice. *J Neurosci* 30: 1947–1967, 2010.

Ohtani Y, Miyata M, Hashimoto K, Tabata T, Kishimoto Y, Fukaya M, Kase D, Kassai H, Nakao K, Hirata T, Watanabe M, Kano M, Aiba A. The synaptic targeting of mGluR1 by its carboxyl-terminal domain is crucial for cerebellar function. *J Neurosci* 34: 2702–2712, 2014.

Ozden I, Dombeck DA, Hoogland TM, Tank DW, Wang SS. Widespread state-dependent shifts in cerebellar activity in locomoting mice. *PLoS One* 7: e42650, 2012.

Ozden I, Lee HM, Sullivan MR, Wang SS. Identification and clustering of event patterns from in vivo multiphoton optical recordings of neuronal ensembles. *J Neurophysiol* 100: 495–503, 2008.

Ozden I, Sullivan MR, Lee HM, Wang SS. Reliable coding emerges from coactivation of climbing fibers in microbands of cerebellar Purkinje neurons. *J Neurosci* 29: 10463–10473, 2009.

Packer AM, Russell LE, Dalgleish HW, Hausser M. Simultaneous all-optical manipulation and recording of neural circuit activity with cellular resolution in vivo. *Nat Methods* 12: 140–146, 2015.

Rahmati N, Owens CB, Bosman LW, Spanke JK, Lindeman S, Gong W, Potters JW, Romano V, Voges K, Moscato L, Koekkoek SK, Negrello M, De Zeeuw CI. Cerebellar potentiation and learning a whisker-based object localization task with a time response window. *J Neurosci* 34: 1949–1962, 2014.

Rochefort C, Arabo A, Andre M, Poucet B, Save E, Rondi-Reig L. Cerebellum shapes hippocampal spatial code. *Science* 334: 385–389, 2011.

Schonewille M, Belmeguenai A, Koekkoek SK, Houtman SH, Boele HJ, van Beugen BJ, Gao Z, Badura A, Ohtsuki G, Amerika WE, Hosy E, Hoebeek FE, Elgersma Y, Hansel C, De Zeeuw CI. Purkinje cell-specific knockout of the protein phosphatase PP2B impairs potentiation and cerebellar motor learning. *Neuron* 67: 618–628, 2010.

Schonewille M, Gao Z, Boele HJ, Veloz MF, Amerika WE, Simek AA, De Jeu MT, Steinberg JP, Takamiya K, Hoebeek FE, Linden DJ, Huganir RL, De Zeeuw CI. Reevaluating the role of LTD in cerebellar motor learning. *Neuron* 70: 43–50, 2011.

Schultz SR, Kitamura K, Post-Uiterweer A, Krupic J, Hausser M. Spatial pattern coding of sensory information by climbing fiber-evoked calcium signals in networks of neighboring cerebellar Purkinje cells. *J Neurosci* 29: 8005–8015, 2009.

Slotnick B. A simple 2-transistor touch or lick detector circuit. *J Exp Anal Behav* 91: 253–255, 2009.

Stosiek C, Garaschuk O, Holthoff K, Konnerth A. In vivo two-photon calcium imaging of neuronal networks. *Proc Natl Acad Sci USA* 100: 7319–7324, 2003.

Sullivan MR, Nimmerjahn A, Sarkisov DV, Helmchen F, Wang SS. In vivo calcium imaging of circuit activity in cerebellar cortex. *J Neurophysiol* 94: 1636–1644, 2005.

Tanaka S, Kawaguchi SY, Shioi G, Hirano T. Long-term potentiation of inhibitory synaptic transmission onto cerebellar Purkinje neurons contributes to adaptation of vestibulo-ocular reflex. *J Neurosci* 33: 17209–17220, 2013.

Tsutsumi S, Yamazaki M, Miyazaki T, Watanabe M, Sakimura K, Kano M, Kitamura K. Structure-function relationships between aldolase C/zebrin II expression and complex spike synchrony in the cerebellum. *J Neurosci* 35: 843–852, 2015.

Vogelstein JT, Packer AM, Machado TA, Sippy T, Babadi B, Yuste R, Paninski L. Fast nonnegative deconvolution for spike train inference from population calcium imaging. *J Neurophysiol* 104: 3691–3704, 2010.

Wang SS, Denk W, Hausser M. Coincidence detection in single dendritic spines mediated by calcium release. *Nat Neurosci* 3: 1266–1273, 2000.

Wang W, Nakadate K, Masugi-Tokita M, Shutoh F, Aziz W, Tarusawa E, Lorincz A, Molnar E, Kesaf S, Li YQ, Fukazawa Y, Nagao S, Shigemoto R. Distinct cerebellar engrams in short-term and long-term motor learning. *Proc Natl Acad Sci USA* 111: E188–E193, 2014.

Welsh JP. Systemic harmaline blocks associative and motor learning by the actions of the inferior olive. *Eur J Neurosci* 10: 3307–3320, 1998.

Welsh JP, Lang EJ, Suglhara I, Llinas R. Dynamic organization of motor control within the olivocerebellar system. *Nature* 374: 453–457, 1995.

Welsh JP, Yamaguchi H, Zeng XH, Kojo M, Nakada Y, Takagi A, Sugimori M, Llinas RR. Normal motor learning during pharmacological prevention of Purkinje cell long-term depression. *Proc Natl Acad Sci USA* 102: 17166–17171, 2005.

Wetmore DZ, Jirenhed DA, Rasmussen A, Johansson F, Schnitzer MJ, Hesslow G. Bidirectional plasticity of Purkinje cells matches temporal features of learning. *J Neurosci* 34: 1731–1737, 2014.

Zariwala HA, Borghuis BG, Hoogland TM, Madisen L, Tian L, De Zeeuw CI, Zeng H, Looger LL, Svoboda K, Chen TW. A Cre-dependent GCaMP3 reporter mouse for neuronal imaging in vivo. *J Neurosci* 32: 3131–3141, 2012.